Supplementary information to the manuscript:
Symmetry considerations and development of pinwheels in visual maps

Ha Youn Lee, Mehdi Yahyanejad, and Mehran Kardar
Department of Physics, Massachusetts Institute of Technology, Cambridge, Massachusetts 02139

I. DENSITY OF ZEROS FOR A FIELD WITH ANISOTROPY

We consider a field $\vec{S} \equiv (S_x(x,y), S_y(x,y))$. Subject to joint rotational invariance of $\vec{S}$ and $\vec{r} \equiv (x,y)$, the most general Gaussian weight is

$$p\left[\vec{S}\right] \propto \exp\left\{-\frac{1}{2}\int \frac{d^2q}{(2\pi)^2} S_\alpha(\vec{q}) S_\beta(-\vec{q}) \left[\lambda^{-1}(q)\frac{q_\alpha q_\beta}{q^2} + \tau^{-1}(q)\left(\delta_{\alpha\beta} - \frac{q_\alpha q_\beta}{q^2}\right)\right]\right\}, \tag{1}$$

where $\vec{S}(\vec{q})$ is the Fourier transform of $\vec{S}(\vec{r})$, $\lambda(q)$ and $\tau(q)$ are longitudinal and transverse contents of the power spectrum, and $\tau(q) = \lambda(q)$ in an isotropic system. The average density of zeros is obtained from[1]

$$n = \left\langle \delta^2(\vec{S})\ \det\ \partial_\alpha S_\beta \right\rangle = \left\langle \delta^2\left(\vec{S}(0)\right)\right\rangle \left\langle \left|\partial_x S_x(0)\partial_y S_y(0) - \partial_x S_y(0)\partial_y S_x(0)\right|\right\rangle . \tag{2}$$

Here the average can be taken at $\vec{r} = 0$ because of translation symmetry. Also, the averages $\partial_\alpha \vec{S}$ are independent since the probability distribution function is invariant under $\vec{S} \to \vec{S} + \vec{C}$. The first average is easily calculated as

$$\left\langle \delta^2\left(\vec{S}(0)\right)\right\rangle = \int \frac{d^2k}{(2\pi)^2} \left\langle e^{i\vec{k}\cdot\vec{S}(0)}\right\rangle = \int \frac{d^2k}{(2\pi)^2} \exp\left[-\frac{k^2}{2}\left\langle \vec{S}(0)\cdot\vec{S}(0)\right\rangle\right]. \tag{3}$$

The variance of $\vec{S}(0)$ is

$$\left\langle \vec{S}(0)\cdot\vec{S}(0)\right\rangle = \int \frac{d^2q d^2q'}{(2\pi)^4} \left\langle S_\alpha(\vec{q}) S_\alpha(\vec{q}')\right\rangle = \int \frac{d^2q d^2q'}{(2\pi)^4} (2\pi)^2 \delta^2(\vec{q}+\vec{q}')\ \left[\lambda(q) + \tau(q)\right], \tag{4}$$

and by inserting Eq. (4) to Eq. (3), we get

$$\left\langle \delta^2\left(\vec{S}\right)\right\rangle = \frac{1}{2\pi}\frac{1}{\int \frac{d^2q}{(2\pi)^2}\left[\lambda(q)+\tau(q)\right]} = \frac{1}{\int dq\ q\left[\lambda(q)+\tau(q)\right]}. \tag{5}$$

As a first step to calculating the average determinant, we consider

$$\begin{aligned}
\langle \partial_i S_\alpha(0)\partial_j S_\beta(0)\rangle &= \int \frac{d^2q}{(2\pi)^2}\frac{d^2q'}{(2\pi)^2}(iq_i)(iq'_j)\left\langle S_\alpha(\vec{q}) S_\beta(\vec{q}')\right\rangle \\
&= \int \frac{d^2q}{(2\pi)^2} q_i q_j \left[\lambda(q)\frac{q_\alpha q_\beta}{q^2} + \tau(q)\left(\delta_{\alpha\beta} - \frac{q_\alpha q_\beta}{q^2}\right)\right] \\
&= \int \frac{d^2q}{(2\pi)^2} q^2 \left[\tau(q)\left(\frac{\delta_{ij}\delta_{\alpha\beta}}{2} - \frac{\delta_{ij}\delta_{\alpha\beta} + \delta_{i\alpha}\delta_{j\beta} + \delta_{i\beta}\delta_{j\alpha}}{8}\right)\right. \\
&\qquad \left. + \lambda(q)\frac{\delta_{ij}\delta_{\alpha\beta} + \delta_{i\alpha}\delta_{j\beta} + \delta_{i\beta}\delta_{j\alpha}}{8}\right] \\
&= \frac{\delta_{ij}\delta_{\alpha\beta}}{4\pi}\int dq q^3 \tau(q) + \frac{\delta_{ij}\delta_{\alpha\beta} + \delta_{i\alpha}\delta_{j\beta} + \delta_{i\beta}\delta_{j\alpha}}{16\pi}\int dq q^3\left(\lambda(q) - \tau(q)\right).
\end{aligned} \tag{6}$$

We next rewrite Eq. (6) as

$$\langle \partial_i S_\alpha \partial_j S_\beta\rangle = \delta_{ij}\delta_{\alpha\beta}\ \kappa + \left(\delta_{ij}\delta_{\alpha\beta} + \delta_{i\alpha}\delta_{j\beta} + \delta_{i\beta}\delta_{j\alpha}\right)\ \mu, \tag{7}$$

where $\kappa = \int dq\ q^3\ \tau(q)/(4\pi)$, and $\mu = \int dq\ q^3\ (\lambda(q) - \tau(q))/(16\pi)$ is zero in an isotropic system. In the isotropic system, each of the four derivatives is an independent variable. However, for $\mu \neq 0$, there are two correlated pairs

$(\partial_x S_x, \partial_y S_y)$, and $(\partial_x S_y, \partial_y S_x)$. For the first pair, we have $\left\langle (\partial_x S_x)^2 \right\rangle = \left\langle (\partial_y S_y)^2 \right\rangle = \kappa + 3\mu$, while for the second pair $\left\langle (\partial_y S_x)^2 \right\rangle = \left\langle (\partial_x S_y)^2 \right\rangle = \kappa + \mu$. The cross correlations in each pair are identical, $\langle \partial_x S_x \partial_y S_y \rangle = \langle \partial_x S_y \partial_y S_x \rangle = \mu$, such that the average value of the determinant is zero.

As a second step towards the calculation of average absolute value of the determinant, we find its probability distribution as

$$p(d) = \langle \delta \left[d - (\partial_x S_x \partial_y S_y - \partial_x S_y \partial_y S_x) \right] \rangle = \int \frac{d\omega}{2\pi} e^{i\omega d} \left\langle e^{i\omega(\partial_x S_x \partial_y S_y - \partial_x S_y \partial_y S_x)} \right\rangle . \tag{8}$$

As established above, the two factors in the final exponent are independent random elements. The random variables $\partial_\alpha S_\beta \equiv u_{\alpha\beta}$ are Gaussian distributed, with co-variances given by Eq. (7). By inverting the co-variance matrix, we can construct the probability distribution for $\{u_{\alpha\beta}\}$, and then calculate the average

$$\begin{aligned}
\left\langle e^{i\omega u_{xx} u_{yy}} \right\rangle &= \int \frac{du_{xx} du_{yy}}{\mathcal{N}} \exp\left\{ -\frac{1}{2}(u_{xx}, u_{yy}) \begin{bmatrix} \frac{\kappa+\mu}{(\kappa+\mu)^2-\mu^2} & -\frac{\mu}{(\kappa+\mu)^2-\mu^2} - i\omega \\ -\frac{\mu}{(\kappa+\mu)^2-\mu^2} - i\omega & \frac{\mu}{(\kappa+\mu)^2-\mu^2} \end{bmatrix} \begin{pmatrix} u_{xx} \\ u_{yy} \end{pmatrix} \right\} \\
&= \left[\frac{(\kappa+\mu)^2}{((\kappa+\mu)^2-\mu^2)^2} - \frac{\mu^2}{((\kappa+\mu)^2-\mu^2)^2} - \frac{2i\omega\mu}{(\kappa+\mu)^2-\mu^2} + \omega^2 \right]^{-\frac{1}{2}} \\
&\quad \times \left[\frac{(\kappa+\mu)^2-\mu^2}{((\kappa+\mu)^2-\mu^2)^2} \right]^{\frac{1}{2}} \\
&= \left[1 + \omega^2((\kappa+\mu)^2 - \mu^2) - 2i\omega\mu \right]^{-\frac{1}{2}} .
\end{aligned} \tag{9}$$

(The normalization $\mathcal{N}$ in the denominator is simply the numerator evaluated at $\omega = 0$.) Similarly, the second average is

$$\left\langle e^{-i\omega u_{xy} u_{yx}} \right\rangle = \left[1 + \omega^2((\kappa+3\mu)^2 - \mu^2) + 2i\omega\mu \right]^{-\frac{1}{2}} . \tag{10}$$

Inserting Eqs. (9) and (10) into Eq. (8) gives the implicit result

$$p(d) = \int_{-\infty}^{\infty} \frac{d\omega}{2\pi} \frac{e^{i\omega d}}{[1 - 2i\omega\mu + \omega^2(\kappa^2 + 2\mu\kappa)]^{\frac{1}{2}} [1 + 2i\omega\mu + \omega^2(\kappa^2 + 6\mu\kappa + 8\mu^2)]^{\frac{1}{2}}}. \tag{11}$$

Let us consider the isotropic case, $\mu = 0$. The probability distribution function is

$$p(d) = \int_{-\infty}^{\infty} \frac{d\omega}{2\pi} \frac{e^{i\omega d}}{1 + \kappa^2\omega^2} = \frac{1}{2\kappa} e^{-|d|/\kappa}, \tag{12}$$

from which we obtain

$$\langle |d| \rangle = 2 \int_0^{\infty} dx \frac{1}{2\kappa} e^{-x/\kappa} = \kappa. \tag{13}$$

From Eqs. (2), (5), and (13), average density of pinwheels is then

$$n = \frac{1}{4\pi} \frac{\int dq q^3 \tau(q)}{\int dq q (\lambda(q) + \tau(q))} = \frac{1}{8\pi} \frac{\int dq q^3 P(q)}{\int dq q P(q)}, \tag{14}$$

where $P(q) = \lambda(q) + \tau(q) = 2\tau(q)$ is the power spectrum of the field. The above result is smaller by a factor of two than that obtained in Ref. [2]. However, our calculation was with a vector field, whereas the orientation preference is a director field which is the same if the vector is inverted. To incorporate this feature, Ref. [2] works with a complex field $|z(\vec{x}|e^{2i\theta(\vec{x})} \equiv (S_x + iS_y)^2$, a procedure that doubles the zeros calculated above for the field $(S_x + iS_y)$. This factor is not important to us, since we are interested in how the result is modified by anisotropy.

Performing the integral in Eq. (11) for $\mu \neq 0$ is not an easy task. We note that since $\langle d \rangle = 0$, the average of the absolute value provides a measure of the width of the probability distribution $p(d)$. A similar measure of the width of the distribution that is much easier to calculate is the standard deviation $\sqrt{< d^2 >}$. Using standard properties of

Gaussian distributed variables, the variance of d is calculated as

$$\begin{aligned}\left\langle d^2\right\rangle &= \left\langle \left(\partial_x S_x \partial_y S_y - \partial_x S_y \partial_y S_x\right)^2 \right\rangle \\ &= \left\langle \left(\partial_x S_x\right)^2 \right\rangle \left\langle \left(\partial_y S_y\right)^2 \right\rangle + 2\left\langle \partial_x S_x \partial_y S_y \right\rangle^2 + \left\langle \left(\partial_x S_y\right)^2 \right\rangle \left\langle \left(\partial_y S_x\right)^2 \right\rangle \\ &\quad +2\left\langle \partial_x S_y \partial_y S_x \right\rangle^2 - 2\left\langle \partial_x S_x \partial_y S_y \right\rangle \left\langle \partial_x S_y \partial_y S_x \right\rangle \\ &= (\kappa+3\mu)^2 + 2\mu^2 + (\kappa+\mu)^2 + 2\mu^2 - 2\mu^2 \\ &= 2\kappa^2 + 8\mu\kappa + 12\mu^2. \end{aligned} \tag{15}$$

As measures of the width of the distribution, $\langle|d|\rangle$ and $\sqrt{\langle d^2\rangle}$ should vary together. For our estimate, we shall assume that they are proportional, and choose the a proportionality constant that makes the two expression equal for $\mu = 0$; i.e. we make the replacement

$$\langle|d|\rangle \to \sqrt{\frac{\langle d^2\rangle}{2}} = \sqrt{\kappa^2 + 4\mu\kappa + 6\mu^2}, \tag{16}$$

resulting in the density of zeros

$$n \approx \frac{\sqrt{\kappa^2 + 4\mu\kappa + 6\mu^2}}{\int dq\ q\ (\lambda(q) + \tau(q))}. \tag{17}$$

Using the expressions for κ and μ, we note that

$$\kappa + 2\mu = \frac{1}{4\pi}\int dq\ q^3\ \left(\tau(q) + \frac{\lambda(q) - \tau(q)}{2}\right) = \frac{1}{8\pi}\int dq q^3 P(q), \tag{18}$$

where $P(q) \equiv \lambda(q) + \tau(q)$ is the total power content at q. With the aid of Eq. (18), Eq. (17) now becomes

$$n \approx \frac{\sqrt{(\kappa+2\mu)^2 + (2\mu)^2}}{\int dq\ q\ P(q)} = \frac{1}{8\pi}\frac{\int dq\ q^3\ P(q)}{\int dq\ q\ P(q)}\sqrt{1 + \left[\frac{\int dq\ q^3\ (\lambda(q) - \tau(q))}{\int dq\ q^3\ (\lambda(q) + \tau(q))}\right]^2}. \tag{19}$$

For a fixed $P(q)$, the density of zeros is minimum in the isotropic limit of $\tau(q) = \lambda(q)$. In the extreme anisotropic limit of $\tau(q) = 0$ or $\lambda(q) = 0$, the density of zeros increases by a factor of $\sqrt{2}$. In view of the approximations involved, we also performed numerical simulations to check if the density of pinwheels is higher in the anisotropic case. We found that this is indeed the case although the relative increase in density of 1.12 is less than the value of $\sqrt{2}$.

Let us illustrate the time evolution of the density of zeros, using a simple linear model for development of the field, in which the longitudinal and transverse components of the power spectrum grow as

$$\begin{aligned}\lambda(q,t) &= \lambda_0(q)\ e^{r_l(q)\ t}, \\ \tau(q,t) &= \tau_0(q)\ e^{r_t(q)\ t}, \end{aligned} \tag{20}$$

where growth rates are $r_l(q) = 2[J(q) + q^2 K(q)]$ and $r_t(q) = 2J(q)$. If initially $\lambda_0(q) = \tau_0(q) = P_0/2$, for $q < q_{\max}$, i.e. an isotropically random initial condition, the density of zeros starts as

$$n(t=0) \approx \frac{1}{16\pi} q_{\max}^2. \tag{21}$$

As time goes on, modes with the largest growth rate dominate, reducing n through pair annihilations. Assuming small anisotropy, such that $r_l(q) \approx r_t(q) = 2J(q)$ with a maximum at $\bar{q} = 2\pi/\Lambda$, we have

$$n\left(t \geq (2J(\bar{q}))^{-1}\right) \approx \frac{1}{8\pi}\bar{q}^2 = \frac{\pi}{2\Lambda^2}. \tag{22}$$

However, because of small anisotropy ($r_l(q) \neq r_t(q)$), one of these nearly degenerate modes will dominate the other, such that for longer times,

$$n\left(t \geq (2\bar{q}^2 K(\bar{q}))^{-1}\right) \approx \frac{1}{8\pi}\bar{q}^2\sqrt{2} = \frac{\pi}{2\Lambda^2}\sqrt{2}. \tag{23}$$

Figure 3 in the manuscript shows schematic evolution of n for isotropic and anisotropic cases, the increase of the density in the latter must also involve creation of pairs of vortices.

II. CORTICAL MAP OF CAT

We also measured joint histograms, $h_R[2(\theta_i-\theta_j), 2(\phi_j-\theta_j)]$ for the map of cat in a manner similar to the monkey. The size of the cat map is 204×372 pixels, each representing a region of linear size 13 micrometers. As in the case of monkey map, we display histograms for short separations of 5 to 10 pixel spacings [Figs. 1(a) and (b)] and separations comparable to pinwheel separations of 55 to 60 [Figs. 1(c) and (d)]. There is no dependence on the relative angle for short distances, but such a dependence appears on distances comparable to pinwheel separations. This again indicates a lack of full rotation symmetry in the map of cat. To estimate errors, we average over 2000 histograms each of which is constructed by random samplings with 2.9% pixels of the cat map.

III. PINWHEEL PATTERNS WITH VARIOUS ANISOTROPIC COUPLINGS

Since we do not claim to know the precise form of interactions that lead to cortical patterns, we should at least show that our conclusions are not sensitive to specific choice of interactions. We tested a variety of long-range interactions in our numerical simulations, and found that pinwheels are generally present in the presence of 'anisotropy.' As an example, we observe a pinwheel pattern with a negative value of K which is used to generate the map in Fig. 2a. Another potential concern is that in our simulations the orientations are represented by a *vector*, while in actuality they should be modelled by a *director* field (vectors without arrows). We also performed simulations in which all angles were explicitly limited to the range from 0 to π. Figure 2b displays the result of such a simulation, once more resulting in a pinwheel pattern (for interaction strength of $K = 0.0039$).

The type of anisotropy introduced above, which couples rotations of orientation and topography, should not be confused with the anisotropy corresponding to preference for a particular direction. In fact, we find that both maps of monkey and cat show a predominance of certain orientations. The histogram of orientations for monkey is shown in Fig. 3a and for cat in Fig. 3b. We test the possibility of stabilizing pinwheels with this form of anisotropy by numerical simulations in models with a preference for the horizontal direction, employing the time evolution

$$\partial_t \vec{s}_i = \vec{s}_i \left(1 - \mid \vec{s}_i \mid^2\right) + \sum_j \left[J\left(r_{ij}\right)\ \vec{s}_j + K\left(r_{ij}\right)\ \ \left(\vec{s}_j \cdot \hat{r}_{ij}\right) \hat{r}_{ij}\right] + \vec{H}, \tag{24}$$

where $\vec{H} = H_x \hat{x}$. Introducing the predominance of certain orientation does not change the outcomes. We still find that with $K(r_{ij}) = 0$, and preference for the horizontal direction with $H_x = 0.1$, results in a rainbow state with no vortices, as depicted in Fig. 4a. We obtain a lattice of pinwheels by adding interactions $K(r_{ij}) = J_l$ with $H_x = 0.1$ [Fig. 4b]. The pinwheels are thus not stabilized by the preference for a particular angle, but by the reduced symmetry of combined rotations of orientations and the visual field.

IV. ERROR ESTIMATION FOR HISTOGRAMS OF ORIENTATION PREFERENCE

We estimate error bars in Fig. 2c and e of the manuscript by averaging over 2000 histograms. Each histogram is calculated by randomly samplings 2.9 % of total pixels in the monkey map. We then tested that this artificial sampling procedure does not lead to spurious effects due to finite-size and other potential factors by applying it to numerically generated maps. For the latter, we generated random pinwheel patterns through superposition of *isotropic* Fourier modes having the same longitudinal and transverse components. To do so, we obtain the orientation at position (i, j) by two-dimensional Fourier transformation of $S_\alpha(\vec{q})(i,j) = \exp(c_1 + c_2 q^2 - c_3 q^4) \exp(i\Phi_{\alpha,i,j})$ where $\alpha = x$ or y and $\Phi_{\alpha,i,j}$ is a random variable ranging from 0 to 2π. Figure 5 displays such an isotropic pattern with 256×256 pixels, with a pinwheel density close to that of the monkey map. The angle histograms from the isotropic pattern for $2\left(\phi_{ij} - \theta_j\right) = 0$ (red line) and $2\left(\phi_{ij} - \theta_j\right) = 90$ (black line) are shown in Fig. 5b. We construct histograms for the isotropic pattern with larger size (512×512) than the monkey map(360×480) [Fig. 5]. Here error bars in Fig. 5b and c are estimated by averaging over 2000 histograms. As in the analysis for the monkey map, each histogram is constructed by randomly sampling 2.9% of total pixels in one pattern. The difference between two histograms for $2\left(\phi_{ij} - \theta_j\right) = 0$ and $2\left(\phi_{ij} - \theta_j\right) = 90$ from the monkey map is larger than the histogram differences form both isotropic patterns with sizes 256×256 and 512×512. Hence we have some confidence that observed couplings of relative

orientation to the underlying topography in the monkey map are not from statistical errors.

[1] Halperin, B. T., in *Physics of Defects, Les Houches Session XXXV, 1980* (eds Balian, R., Kléman, M. & Poirir, J.-P.) 813-857 (North Holland, Amsterdam, 1981).
[2] F. Wolf and T. Geisel, Spontaneous pinwheel annihilation during visual development. Nature **395**, 73-78 (1998).

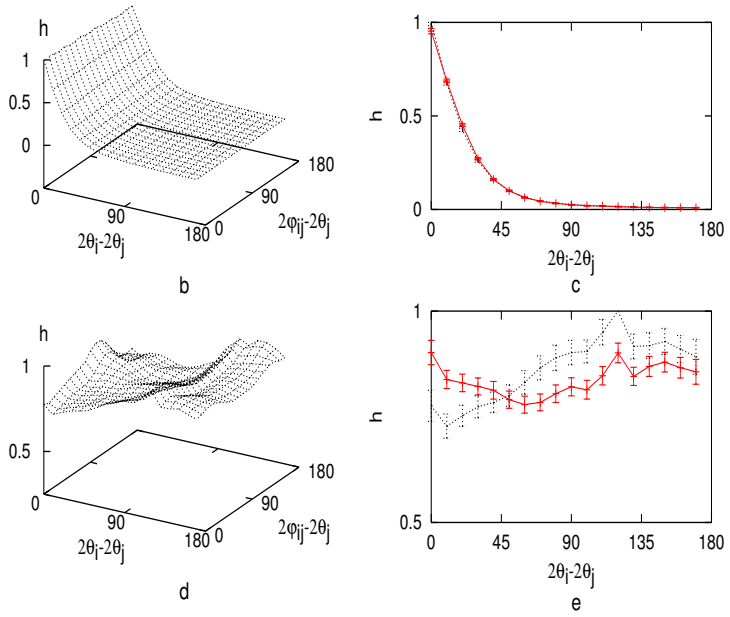

FIG. 1: Histograms of OP from a map of cat. Here $\theta_i(\theta_j)$ is the preferred orientation at a pixel $i(j)$, and ϕ_{ij} is the angle of the line joining points i and j. The left column displays full histograms as functions of relative orientations, as well as orientations relative to the line joining the two pixels i and j. In the right column, solid lines represent histograms for $2(\phi_{ij} - \theta_j) = 0^o$, and dotted lines represent histograms for $2(\phi_{ij} - \theta_j) = 90^o$. **a** and **b** correspond to separations of 5 to 10 pixel spacings, and **c** and **d** to separations of 55 to 60 pixels.

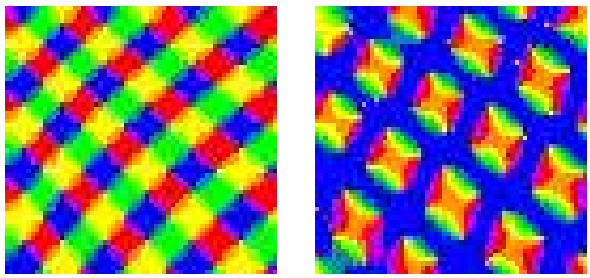

FIG. 2: **a.** Stable pattern of pinwheels with joint rotation symmetry, with a negative value of $K = -0.0039$. (Compare with Fig. 4c of the manuscript.) **b.** A pinwheel pattern is also generated in simulations where the angles are constrained to the region of $[0,\pi]$.

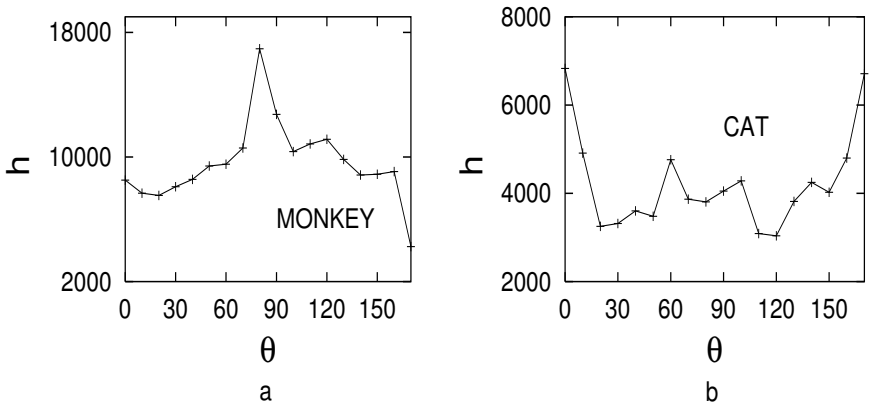

FIG. 3: Predominance of certain orientation in the maps of monkey (a) and cat (b). All orientations are not equally present in either map.

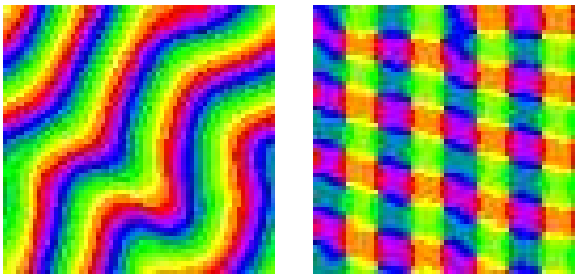

a b

FIG. 4: **a.** The development of a random initial condition by a filter with isotropic pair interactions ($K(r_ij) = 0$), but with a preference for the horizontal direction ($H_x = 0.1$). Such preference does not stabilize the pinwheels. **b.** The stabilized pinwheel pattern with anisotropic pairwise interactions ($K(r_{ij}) = -0.0039$), in addition to a preference for the horizontal direction ($H_x = 0.1$).

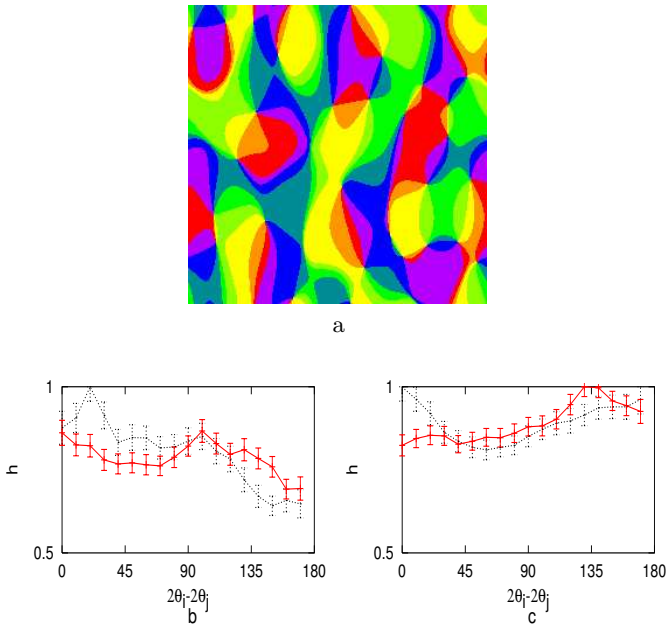

FIG. 5: **a.** A pinwheel pattern randomly generated by superposition of isotropic Fourier modes. The size of the pattern is 256×256 pixels. The relative angle histograms for $2(\phi_{ij} - \phi_j) = 0^o$ (black) and $2(\phi_{ij} - \phi_j) = 90^o$ (red) from patterns with sizes of 256×256 (b) and 512×512 (c). Here error bars are estimated by averaging over 2000 histograms. Neither pattern shows comparable topographic dependence to that in the monkey map.